Journal of Solid State Chemistry 183 (2010) 2995–3001

Contents lists available at ScienceDirect

Journal of Solid State Chemistry

journal homepage: www.elsevier.com/locate/jssc

3D [Ag–Mg] polyanionic frameworks in the $La_4Ag_{10}Mg_3$ and $La_4Ag_{10.3}Mg_{12}$ new ternary compounds

Pavlo Solokha [a,*], Serena De Negri [a], Volodymyr Pavlyuk [b,c], Bernhard Eck [d], Richard Dronskowski [d], Adriana Saccone [a]

[a] Department of Chemistry and Industrial Chemistry, University of Genoa, Str. Dodecaneso 31, I-16146 Genova, Italy
[b] Department of Inorganic Chemistry, Ivan Franko National University of Lviv, Kyryla and Mefodiya str. 6, 79005 Lviv, Ukraine
[c] Institute of Chemistry and Environment Protection, Jan Dlugosz University, al. Armii Krajowej 13/15, 42200 Czestochowa, Poland
[d] Institut für Anorganische Chemie, RWTH Aachen University, 52056 Aachen, Germany

ARTICLE INFO

Article history:
Received 30 July 2010
Received in revised form
9 October 2010
Accepted 11 October 2010
Available online 20 October 2010

Keywords:
3D-frameworks
Intermetallics
Crystal structure
Chemical bonding

ABSTRACT

The crystal structures of two new ternary phases, $La_4Ag_{10}Mg_3$ and $La_4Ag_{10.3}Mg_{12}$, were refined from X-ray single crystal diffraction data. $La_4Ag_{10}Mg_3$ crystallizes in the $Ca_4Au_{10}In_3$ structure type, an ordered variant of the binary Zr_7Ni_{10} compound: orthorhombic, *Cmce*, *oS*68, $a=14.173(5)$, $b=10.266(3)$, $c=10.354(3)$ Å, $Z=4$, w$R_2=0.0826$, 676 F^2 values, 50 variables. $La_4Ag_{10.3}Mg_{12}$ represents a new structure type: orthorhombic, *Cmmm*, *oS*116-10.32, $a=9.6130(3)$, $b=24.9663(8)$, $c=9.6333(2)$ Å, $Z=4$, w$R_2=0.0403$, 1185 F^2 values, 101 variables. The structural analysis of both compounds, highlighting a significant contraction of the Ag–Mg distances, suggests the existence of three-dimensional [Ag–Mg] networks hosting La atoms. LMTO calculations applied to $La_4Ag_{10}Mg_3$ indicate that the strongest bonds occur for Ag–Ag and Ag–Mg interactions, and confirm the presence of a $3D_\infty[Ag_{10}Mg_3]^{\delta-}$ polyanionic framework balanced by positively charged La atoms.

1. Introduction

A very interesting class of intermetallic phases is represented by polar intermetallics in which polyanionic networks, formed by one or two types of atoms, are combined with electropositive metals, mainly belonging to the groups 1 and 2 and to the rare-earth elements (R) series. Differently from classical Zintl phases, in polar intermetallics atoms forming the polyanionic network do not necessarily follow simple valence rules for bonding and their nature is therefore not strictly limited by the "Zintl border", originally placed between the groups 13 and 14. In fact many polar binary and ternary intermetallic phases were discovered containing both late transition metals or/and early post-transition elements (such as Al, In, Si, Ge) [1,2]. The investigation of crystal structures and chemical bonding in these materials could contribute to a deeper knowledge of the chemistry of metal-based systems. In a recent overview on polar intermetallics the Au tendency to strongly bond with elements such as In, Tl and Sn forming polyanionic networks is discussed [1]. The possibility of substitutions of In by Mg or Zn in the same structure is also mentioned, on the basis of their electronegativity values. Actually, chemical bonding studies on the EuAuMg phase had evidenced that in this structure gold and magnesium form a three-dimensional network [3]. In the same article the isostructural EuAgMg phase had also been investigated, and it was presented as a $[AgMg]^{\delta-}$ covalent network separated and balanced by Eu atoms. Following these results and considering the high reactivity of magnesium with rare earth metals and late transition elements, the *R*–Ag–Mg systems seem potential hunting-grounds for discovering new polar intermetallic phases. During the investigation of phase relationships in the La–Ag–Mg system several new ternary phases were in fact found [4]. In this paper crystal structure and chemical bonding studies on $La_4Ag_{10}Mg_3$ and $La_4Ag_{10.3}Mg_{12}$ are presented.

2. Experimental section

2.1. Synthesis

Two alloys of nominal compositions $La_{26}Ag_{59}Mg_{15}$ and $La_{20}Ag_{42}Mg_{38}$ were prepared from the compact elemental metals, all with nominal purities >99.9 wt%. Lanthanum and Silver were supplied by Newmet Koch, Waltham Abbey, England, Magnesium by MaTecK, Jülich, Germany.

The $La_{26}Ag_{59}Mg_{15}$ sample was synthesized in Ar atmosphere by induction melting the proper amounts of constituent elements enclosed in a Ta crucible closed by an arc-sealed lid. The crucible was being shaken during the melting procedure, which was

* Corresponding author. Fax: +39 0103538733.
E-mail address: solokha.pavlo@chimica.unige.it (P. Solokha).

0022-4596/$ - see front matter © 2010 Elsevier Inc. All rights reserved.
doi:10.1016/j.jssc.2010.10.018

repeated at least three times as to ensure the homogeneity of the alloy. After, the sample was annealed for a month at 400 °C in a resistance furnace by placing the Ta crucible in a sealed quartz phial.

Single crystals extracted from an induction melted $La_{20}Ag_{42}Mg_{38}$ sample were of poor quality, so a new sample was prepared on this composition by using a different procedure: an arc-sealed Ta-crucible containing stoichiometric amounts of the constituent elements was placed in an evacuated quartz vial, and then located in a resistance furnace equipped with a thermal cycle controller. The reaction mixture was stepwise heated to 700 °C (5 °C/min), held at this temperature for 15 min, and slowly cooled (0.1 °C/min) to 350 °C; after the furnace was switched off and the sample was cooled to room temperature.

After treatment, samples could easily be separated from the tantalum container. No side-reaction of the alloys with the crucible was detected. The samples were stable against air and moisture as compact buttons as well as fine-grained powders.

2.2. Microstructure and phase analysis

Samples characterization was carried out by a scanning electron microscope (*EVO 40*, Carl Zeiss SMT Ltd, Cambridge, England) equipped with a Pentafet Link energy-dispersive X-ray spectroscopy (EDXS) system. Microstructure was observed and phase compositions measured. A smooth surface of specimens was prepared by using SiC papers and diamond pastes down to 1 μm grain size. Cobalt standard was used for calibration. X-ray spectra were processed by the software package INCA Energy (Oxford Instruments, Analytical Ltd., Bucks, UK).

2.3. X-ray diffraction measurements

Single crystals of good quality with metal luster and size suitable to perform single crystal measurements ($La_4Ag_{10}Mg_3$ crystal has a prism form of $0.1 \times 0.07 \times 0.05\ mm^3$; $La_4Ag_{10.3}Mg_{12}$ crystal has a plate form of $0.15 \times 0.13 \times 0.03\ mm^3$) were extracted from the mechanically crushed alloys of a button compact form. The crystals were mounted on glass fibers using quick-drying glue. Intensity data have been collected on a Bruker Kappa APEXII CCD area-detector diffractometer by using the graphite monochromatized Mo$K\alpha$ radiation ($\lambda = 0.71073$ Å) in ω scan mode at room temperature. The complete data sets were collected over the reciprocal space up to $\sim 26°$ in θ and with exposures of 25 s per frame. Data were corrected for absorption using ψ scan method [5]. The structures were solved and refined by full-matrix least-squares procedures on $|F^2|$ using SHELX-97 software package [6,7]. X-ray diffraction on powderized samples was performed by means of a diffractometer Philips *X'Pert* MPD (Cu$K\alpha$ radiation, step mode of scanning) in order to ensure crystal structures of the studied phases.

2.4. Electronic structure calculations

Electronic structure calculations on $La_4Ag_{10}Mg_3$ were performed using the linear muffin-tin orbital (LMTO) method [8–10] in its tight-binding representation [11] which corresponds to a fast linearized form of the Korringa–Kohn–Rostoker (KKR) method [12,13]. The calculations using basis sets composed of short-ranged atom-centered TB-LMTOs without empty spheres were carried out using the TB-LMTO-ASA 4.7 program with a scalar-relativistic Hamiltonian and the atomic-spheres approximations [14]. Electronic energies were calculated via density-functional theory (DFT) based on the local-density approximation (LDA) for the exchange-correlation functional as parametrized by von Barth and Hedin [15]. Diagonalization and integration in reciprocal space were performed with the help of an improved tetrahedron method [16]. In order to evaluate various orbital interactions, density of states (DOS), the crystal orbital Hamilton populations (COHP) curves [17], and the integrated COHP values (*i*COHPs) were also calculated. The electronic structure calculations were carried out using the nonspin-polarized (nonmagnetic) approach, with enough dense *k*-points mesh in the irreducible Brillouin zones of the crystallographic unit cell. All calculations were checked for convergence of energies and COHP with respect to the number of *k* points. From the calculations a mapping of the electrons within the real space was obtained using the electron-localization function (ELF) [18]. All the figures and graphics concerning electron structure calculations were generated by wxDragon [19].

3. Results and discussion

3.1. SEM–EDXS characterization

No impurity elements were detected in the samples, whose measured gross compositions correspond to the nominal ones.

Table 1
Selected crystallographic data and structure refinement parameters for $La_4Ag_{10}Mg_3$ and $La_4Ag_{10.3}Mg_{12}$ single crystals.

Empirical formula	**$La_4Ag_{10}Mg_3$**		**$La_4Ag_{10.3}Mg_{12}$**
EDXS composition	$La_{25.4}Ag_{58.3}Mg_{16.3}$		$La_{15.3}Ag_{39.7}Mg_{45.0}$
Formula weight (g/mol)	1707.27		1968.65
Radiation, wavelength (Å)	Mo$K\alpha$, $\lambda = 0.71073$		Mo$K\alpha$, $\lambda = 0.71073$
Crystal system	orthorhombic		orthorhombic
Space group, *Z*	*Cmce*, 4 (centro)	*Aea*2, 4 (non-centro)	*Cmmm*, 4
Pearson symbol	*oS*68		*oS*116-10.32
Unit cell			
a (Å)	14.173(5)	10.354(2)	9.6130(3)
b (Å)	10.266(3)	10.266(2)	24.9663(8)
c (Å)	10.354(3)	14.173(3)	9.6333(2)
V (Å^3)	1506.5(8)	1506.5(8)	2312.0(1)
Density (ρ_{calc}) (g/cm^3)	7.527	7.527	5.66
Abs. coeff. (μ), (mm^{-1})	23.815	23.815	16.095
Ref. data/params	676/50	852/90	1185/101
Flack parameter	–	0.0(3)	–
GOF on F^2	1.090	1.04	1.107
R_1/wR_2[a] [$I > 2\sigma(I)$]	0.0385/0.0826	0.0364/0.0783	0.0205/0.0403
(all data)	0.0640/0.0905	0.0666/0.0883	0.0317/0.0427
Max. residual peaks (e/Å^3)	1.61/−1.79	1.88/−1.78	0.94/−0.97

[a] $R_1 = \sum||F_o| - |F_c||/\sum|F_o|$, $wR_2 = [\sum[w[F_o^2 - F_c^2]2]/\sum[w[F_o^2]2]]^{1/2}$, and $w = 1/[\sigma^2 F_o^2 + [AP]^2 + BP]$, $P = [F_o^2 + 2F_c^2]/3$. *A* and *B* are weight coefficients.

The alloy with nominal composition $La_{26}Ag_{59}Mg_{15}$ is almost single phase; the measured composition of this phase is $La_{26.7}Ag_{58.9}Mg_{14.4}$. In the alloy with nominal composition $La_{20}Ag_{42}Mg_{38}$ dark grey crystals of $La_4Ag_{10.3}Mg_{12}$ were identified, whose measured composition is $La_{15.2}Ag_{40.0}Mg_{44.8}$. Three more phases are present in this sample: $La(Ag_xMg_{1-x})_3$ (structure type BiF_3–*cF*16) with composition $La_{26.1}Ag_{45.8}Mg_{28.1}$ and two other La–Ag–Mg ternary phases of $La_{21}Ag_{43}Mg_{36}$ and $La_{17}Ag_{26}Mg_{57}$ compositions. The indicated phase compositions are values averaged on at least six EDXS measurements. Two microstructure images of these alloys are available in Fig. 1S and 2S (supplementary material).

3.2. Structure determination and refinement

Selected crystallographic data and structure refinement parameters for the studied phases are listed in Table 1. Details on the structure refinement can be found also in CIF files deposited with Fachinformationszentrum Karlsruhe, 76344 Eggenstein-Leopoldshafen, Germany: depository numbers CSD-421583 ($La_4Ag_{10}Mg_3$) and CSD-421582 ($La_4Ag_{10.3}Mg_{12}$). The theoretical powder patterns generated from the single crystal models correspond well to the observed powder diffraction patterns.

3.2.1. $La_4Ag_{10}Mg_3$

Only $h+k=2n$ reflections were observed in the recorded data set clearly indicating that this crystal structure possesses a *C*-centered orthorhombic unit cell. The test of statistical distribution of intensities $|E^2-1|$ gives 0.806 with no strong indication of centrosymmetrical character. The intensity pattern and systematic absences are consistent with the orthorhombic space groups *Cmca* and *Aba*2 (further referred as *Cmce* and *Aea*2 according to new standard entries in International Tables for Crystallography [20]). The structure solution was tried in the centrosymmetric *Cmce* space group and a structural model consisting of 7 independent positions was easily deduced by direct methods using SHELX-97 software [6,7]. Considering the interatomic distances the positions were assumed to be 2 La, 3 Ag and 2 Mg sites. The U_{eq} values of Mg sites were significantly lower than those of other atom types, suggesting the partial presence of a heavier atom in these positions. Taking also into account the EDXS analysis data, a La/Mg mixture was assumed in both these positions. The occupancy parameters were varied in a separate series of least-squares cycles along with the displacement parameters also for other crystallographic sites, but all of them did not vary noticeably from 100% and were assumed to be unity in further cycles. At the end, the final model was refined anisotropically and converged at $R_1=3.85\%$, $wR_2=8.26\%$ and GOF=1.09 with a flat difference Fourier map. According to the Pearson's Crystal Data compilation [21] the binary Zr_7Ni_{10} compound possesses the same structure type. Firstly, the structure of Zr_7Ni_{10} was stated to be non-centrosymmetric, crystallizing in the *Aea*2 space group [22]. Later [23], the same binary phase was re-checked and the centrosymmetric *Cmce* space group was stated to be the correct one. To be sure of the obtained model for the studied ternary phase, we also performed a refinement in *Aea*2 space group. Although, the obtained reliability factors are of similar values (see Table 1), so the $La_4Ag_{10}Mg_3$ compound was considered to crystallize in the centrosymmetric *Cmce* space group (because of small percentages of La in Mg sites, further we will refer to this compound as stoichiometric). Nonetheless, the first ternary representative of Zr_7Ni_{10} type is $Ca_4Au_{10}In_3$, discovered by Lin and Corbett [24].

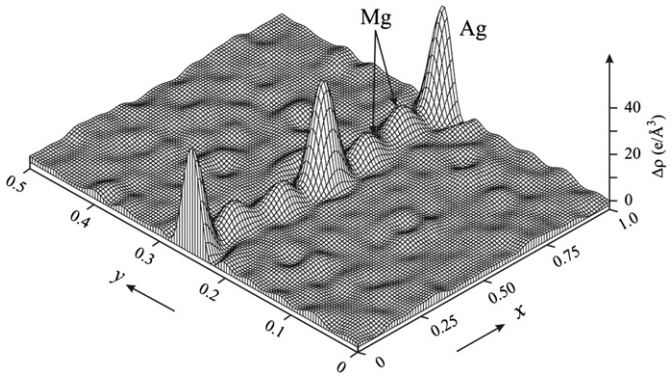

Fig. 1. Difference Fourier map of $La_4Ag_9Mg_{12}$ (preliminary model of $La_4Ag_{10.3}Mg_{12}$) in the region $0\le x\le 1$, $0\le y\le 0.5$ and $z=0$.

3.2.2. $La_4Ag_{10.3}Mg_{12}$

A careful analysis of systematic absences for this data set clearly indicates a base centered orthorhombic unit cell and the following plausible space groups: *C*222 (no. 21), *Cmmm* (no. 65), *Cmm*2 (no. 35) and *C*2*mm* (no. 38). The last two were not taken into account because of highly elevated CFOM (combined figure of merit) values. Intensity statistic ($|E^2-1|=0.946$) favored the centrosymmetric space group *Cmmm*. The major part of starting atomic parameters was deduced from an automatic interpretation of direct methods followed by difference Fourier syntheses using *SHELX-97* package programs. Taking into account the interatomic distances and isotropic displacement parameters, the preliminary structural model was assumed to contain 3 La, 7 Ag, and 5 Mg sites (in the final model—completely occupied sites). Nonetheless, three additional prominent peak maxima along the (100) direction at *x*, ~1/4, 0 with *x*=0, 0.17, and 0.25 were found. A relief mode representation of the difference Fourier map from $0\le x\le 1$, $0\le y\le 0.5$ and $z=0$ is shown in Fig. 1.

Also, the possibility of non-merohedral twinning was checked by TwinRotMat implemented in *PLATON* [25], but it did not result any reasonable twinning for this data set. Because of the chemically impossible short distances between these peaks and the already

Table 2
Atomic coordinates and equivalent isotropic displacement parameters (Å^2) for the $La_4Ag_{10}Mg_3$ single crystal.

Atom	Wyckoff position	Site	*x/a*	*y/b*	*z/c*	U_{eq}[a]	SOF
La1	8*f*	*m*..	0	0.30287(12)	0.20211(13)	0.0138(4)	1
La2	8*d*	2..	0.29651(10)	0	0	0.0148(4)	1
Ag1	8*f*	*m*..	0	0.09649(15)	0.40526(16)	0.0139(4)	1
Ag2	16*g*	1	0.13785(10)	0.03587(12)	0.20571(12)	0.0198(4)	1
Ag3	16*g*	1	0.36457(11)	0.29533(12)	0.02799(13)	0.0214(4)	1
Mg1 La	4*a*	2/*m*..	0	0	0	0.019(2)	0.94(1)
Mg2 La	8*e*	.2.	1/4	0.2699(6)	1/4	0.025(8)	0.92(1)

[a] U_{eq} is defined as one-third of the trace of the orthogonalized U_{ij} tensor.

defined atomic positions the occupancy was allowed to refine freely in further cycles for these sites (the highest peak at 0, ~1/4, 0 was assigned to be Ag, the other peaks—Mg atoms). After that, the residuals dropped drastically, the sum of the mentioned partially occupied Ag7, Mg7 and Mg8 sites gave 1.05. Further, the sum of the occupation factors for them was fixed to be unity. We note that a similar behavior of Ag–Mg "disordering" (including one Ag and two Mg sites) was recently studied for the binary γ-$AgMg_4$ compound [26] and related crystal structures with similar disorder phenomena were predicted to exist. Nonetheless, such a disordered model of the crystal structure was not yet satisfying because some isotropic thermal parameters deviated noticeably from others and the composition of the phase did not match well with EDXS data. As a check for the correct composition, the site occupancy factors (SOF) were varied in a separate series of least-squares cycles along with the displacement parameters. The occupancies did not vary noticeably and were always close to 100% for the La positions. Instead, for some Ag and Mg SOF values deviated remarkably, therefore in the final model an Ag/Mg statistical mixture was assigned for these positions. What is interesting, the presence of Ag/Mg mixture is quite common for Ag–Mg phases i.e. ε-$Ag_{7+x}Mg_{26-x}$ [27], (AgMg), (Ag). In the end, all the atoms were refined anisotropically (for the atom types that are statistically distributed some constraints were used, i.e. EXYZ and EADP command in SHELX; for Mg7 and Mg8 atoms that "play" the same role in crystal structure the SIMU restrain was applied). The assumed model converged at $R_1=2.05\%$, $wR_2=4.03\%$ and GOF=1.107. The residual peaks in the final difference Fourier map of this compound were flat (0.94 and −0.97 e/Å^3, respectively). The details of the data collection and refinement are summarized in Table 1.

3.3. Crystal structure and chemical bonding analysis

3.3.1. $La_4Ag_{10}Mg_3$

The base-centered crystal unit cell consists of 68 atoms distributed among 7 Wyckoff sites. Two general positions are occupied by Ag2 and Ag3 atoms; other species are located on special symmetry sites. Refined positional parameters standardized by *STRUCTURE TIDY* program [28] are shown in Table 2. Interatomic distances within the first coordination sphere are listed in Table 3 for each atom type. It can be noted that the shortest interatomic distances Ag–Mg are significantly contracted with respect to the metallic radii sum (3.04 Å), suggesting a strong interaction between these atoms. The coordination polyhedra of the atoms are strongly distorted and they do not fit well in the classification proposed by Kryp'yakevitch [29]; a more satisfying description of the structure can be obtained considering all the Ag and Mg atoms forming a 3D network, with La atoms embedded into spacious cages inside it. An independent fragment which allows constructing the whole framework by translation is shown in Fig. 3a. The distinctive feature of this framework is a complex unit of simple four connected [Ag_2Mg_2] faces.

The same type of 3D framework, formed by Au and In atoms, was depicted by Lin and Corbett [24] in the structure of $Ca_4Au_{10}In_3$ polar intermetallic. These authors emphasized the sinusoidal layers of Au atoms within the Au–In framework; similar Ag sinusoidal layers can be outlined in $La_4Ag_{10}Mg_3$.

In order to confirm the existence of the 3D [Ag–Mg] network, the electronic structure of $La_4Ag_{10}Mg_3$ was computed ab-initio using the experimental data listed in Table 2 (the small La/Mg mixture was neglected). The Fermi level E_F lies in a continuous DOS region ($n(E_F)=197$) indicating a metallic character for the title compound. Fig. 2a shows the densities of states (DOS) of $La_4Ag_{10}Mg_3$ calculated by the TB–LMTO–ASA method. The DOS in the valence band (VB) exhibits significant silver character giving a wide prominent peak from ~ −6 to −4 eV, while in the conduction band (CB) the empty La states give two peaks at ~3 (E_{La1}) and ~3.5 eV (E_{La2}). The latter behavior is related with the fact that La occupies two symmetry sites not equivalent from the crystallographic point of view as well as with the energy difference influenced by different interactions of La atoms with atoms from the closest coordination sphere. Instead, the site projected DOS of Ag2 and Ag3 (Fig. 2b) are totally superimposed, reflecting identical symmetry of the occupied positions and atomic environment for both of them. From the similar features of DOS running along VB and CB the presence of covalent effects is expected (Table 4).

The electronic structure of $Ca_4Au_{10}In_3$ was calculated by Lin and Corbett [24]; from the comparison of the DOS plots of the two

Table 3
Interatomic distances (Å) within the first coordination spheres calculated with the lattice parameters taken from X-ray single crystal data, and corresponding integrated crystal orbital Hamilton populations (*i*COHP) at E_F for $La_4Ag_{10}Mg_3$. All −*i*COHP values are in eV per bond per cell.

Central atom	Adjacent atoms	δ (Å)	−*i*COHP (eV)	Central atom	Adjacent atoms	δ (Å)	−*i*COHP (eV)	Central atom	Adjacent atoms	δ (Å)	−*i*COHP (eV)
La1–	1Ag1	2.986(2)	0.70	**La2–**	2Ag3	3.116(2)	0.50	**Mg1–**	4Ag3	2.861(2)	0.79
	1Ag1	3.213(2)	0.64		2Ag2	3.119(2)	0.49		4Ag2	2.914(1)	0.77
	2Ag3	3.221(2)	0.63		2Ag3	3.195(2)	0.58		2La1	3.689(2)	0.27
	2Ag2	3.233(2)	0.64		2Ag1	3.203(2)	0.58		2La1	3.748(2)	0.25
	1Ag1	3.243(2)	0.61		2Ag2	3.207(2)	0.57	**Mg2–**	2Ag3	2.826(2)	0.91
	2Ag2	3.366(2)	0.53		2Mg2	3.566(4)	0.40		2Ag2	2.917(5)	0.86
	2Ag3	3.391(2)	0.52						2Ag2	3.193(5)	0.68
	2Mg2	3.594(1)	0.41						2Ag3	3.372(2)	0.54
	1Mg1	3.689(2)	0.27						2La2	3.566(4)	0.40
	1Mg1	3.748(2)	0.25						2La1	3.594(1)	0.41
Ag1–	1Ag1	2.788(2)	1.10	**Ag2–**	1Ag1	2.911(2)	0.92	**Ag3–**	1Mg2	2.826(2)	0.91
	2Ag3	2.886(2)	0.94		1Mg1	2.914(1)	0.77		1Mg1	2.861(2)	0.79
	2Ag2	2.911(2)	0.92		1Mg2	2.917(5)	0.86		1Ag1	2.886(2)	0.94
	1La1	2.986(2)	0.70		1Ag3	2.976(2)	0.72		1Ag2	2.976(2)	0.72
	2La2	3.203(2)	0.58		1Ag3	3.080(2)	0.62		1Ag2	3.080(2)	0.62
	1La1	3.213(2)	0.64		1La2	3.119(2)	0.49		1La2	3.116(2)	0.50
	1La1	3.243(2)	0.61		1Mg2	3.193(5)	0.68		1La2	3.195(2)	0.58
					1La2	3.207(2)	0.57		1La1	3.221(2)	0.63
					1La1	3.233(2)	0.64		1Mg2	3.372(2)	0.54
					1Ag2	3.309(2)	0.43		1La1	3.391(2)	0.52
					1La1	3.366(2)	0.53		1Ag3	3.428(2)	0.37

compounds it appears that the transition element plays the same role in both cases.

The chemical bonding in intermetallic compounds can be effectively visualized by means of the electron localization function (ELF) mapping, which is shown in Fig. 3a and b for the 1/2, 0, 0 crystallographic plane of the $La_4Ag_{10}Mg_3$ structure. The blue regions indicate zero electrons localization; they are distributed around La atoms, indicating that they are positively polarized. The electrons concentration is higher around Mg atoms (towards Ag) and between Ag1–Ag1 dumbbells (red regions). This is also highlighted by the isosurfaces of electron localization function ($\eta=0.8$) around the cited atom types (Fig. 3a). The rest of the $La_4Ag_{10}Mg_3$ crystal space has free electrons-like behavior (green region). These features confirm that the structure of $La_4Ag_{10}Mg_3$ can be conveniently described as formed by a 3D covalent polyanionic $_\infty[Ag_{10}Mg_3]^{\delta-}$ network whose charge is balanced by La atoms.

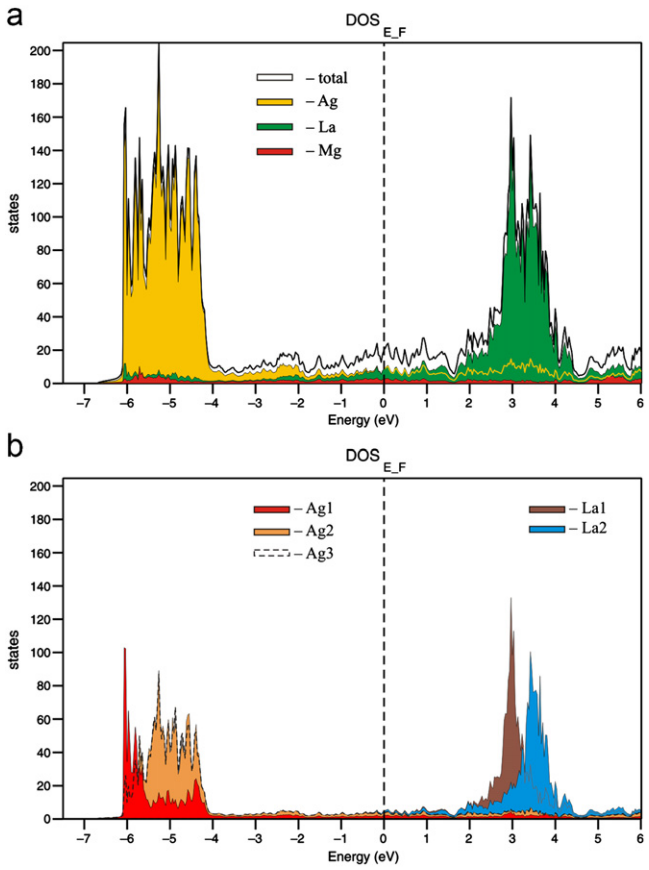

Fig. 2. (a) Total and projected DOS for $La_4Ag_{10}Mg_3$ and (b) site projection of the Ag and La partial DOS of $La_4Ag_{10}Mg_3$.

In order to obtain a quantitative evaluation of the bonding strength between the different types of atoms in the studied structure the COHP and *i*COHP were calculated (Fig. 4, Table 3). Positive values in the –COHP curves represent bonding interactions, negative values indicate antibonding ones: in our case all interactions are of bonding type all over the VB. From the –COHP curves it results that the weakest interactions are La–La and La–Mg. The strongest bonds, indicating a covalent contribution, form between Ag–Ag and Ag–Mg atoms (see also $-i$COHP values in Table 3). This fact is also reflected by their interatomic distances, contracted with respect to the metallic radii sum. Similar features of the COHP curves were obtained for $Ca_4Au_{10}In_3$ [24] where the strongest interactions are Au–Au and Au–In. However, some differences exist between these isostructural compounds:

- the Ca–Au interactions are somewhat weaker than the corresponding La–Ag
- the Au–Au interactions show a strong antibonding counterpart below E_F (suggesting a filled *d*-band), instead in our case the Ag–Ag interactions remain of the bonding type up to E_F.

3.3.2. $La_4Ag_{10.3}Mg_{12}$

In the base centered orthorhombic unit cell of this structure atoms are distributed among 17 Wyckoff sites. Interatomic distances within $La_4Ag_{10.3}Mg_{12}$ are available in the Supplementary Material (Table S2). Similarly to $La_4Ag_{10}Mg_3$ the analysis of

Table 4
Atomic coordinates and equivalent isotropic displacement parameters (Å^2) for the $La_4Ag_{10.3}Mg_{12}$ single crystal.

Atom	Wyckoff position	Site	*x/a*	*y/b*	*z/c*	U_{eq}[a]	SOF
La1	4*i*	*m*2*m*	0	0.38157(3)	0	0.0154(2)	1
La2	4*h*	2*mm*	0.31555(9)	0	1/2	0.0204(2)	1
La3	8*n*	*m*..	0	0.18347(2)	0.28880(6)	0.0171(2)	1
Ag1	8*n*	*m*..	0	0.40449(3)	0.34429(7)	0.0152(2)	1
Ag2	4*k*	*mm*2	0	0	0.2598(1)	0.0202(3)	1
Ag3	4*g*	2*mm*	0.23958(11)	1/2	0	0.0186(2)	1
Ag4	4*f*	..2/*m*	1/4	1/4	1/2	0.0159(4)	0.777(4)
Mg							
Ag5	8*q*	..*m*	0.24769(9)	0.13157(4)	1/2	0.0149(3)	0.739(3)
Mg							
Ag6	8*p*	..*m*	0.16917(8)	0.14959(3)	0	0.0201(3)	0.974(3)
Mg							
Mg1	16*r*	1	0.2261(2)	0.07520(9)	0.2226(2)	0.0176(5)	1
Mg2	4*l*	*mm*2	0	1/2	0.1788(4)	0.0124(9)	1
Mg3	4*i*	*m*2*m*	0	0.06045(18)	0	0.0143(10)	1
Mg4	4*j*	*m*2*m*	0	0.06561(18)	1/2	0.0147(10)	1
Mg5	16*r*	1	0.15953(9)	0.30756(4)	0.24509(9)	0.0185(4)	0.59(2)
Ag							
Mg6	4*j*	*m*2*m*	0	0.30399(15)	1/2	0.0200(15)	0.93(4)
Ag							
Ag7	4*i*	*m*2*m*	0	0.25439(12)	0	0.044(1)	0.453(5)
Mg7	8*p*	..*m*	0.1677(17)	0.2532(6)	0	0.038(6)	0.42(2)
Mg8	4*e*	..2/*m*	1/4	1/4	0	0.045(19)	0.13(2)

[a] U_{eq} is defined as one-third of the trace of the orthogonalized U_{ij} tensor.

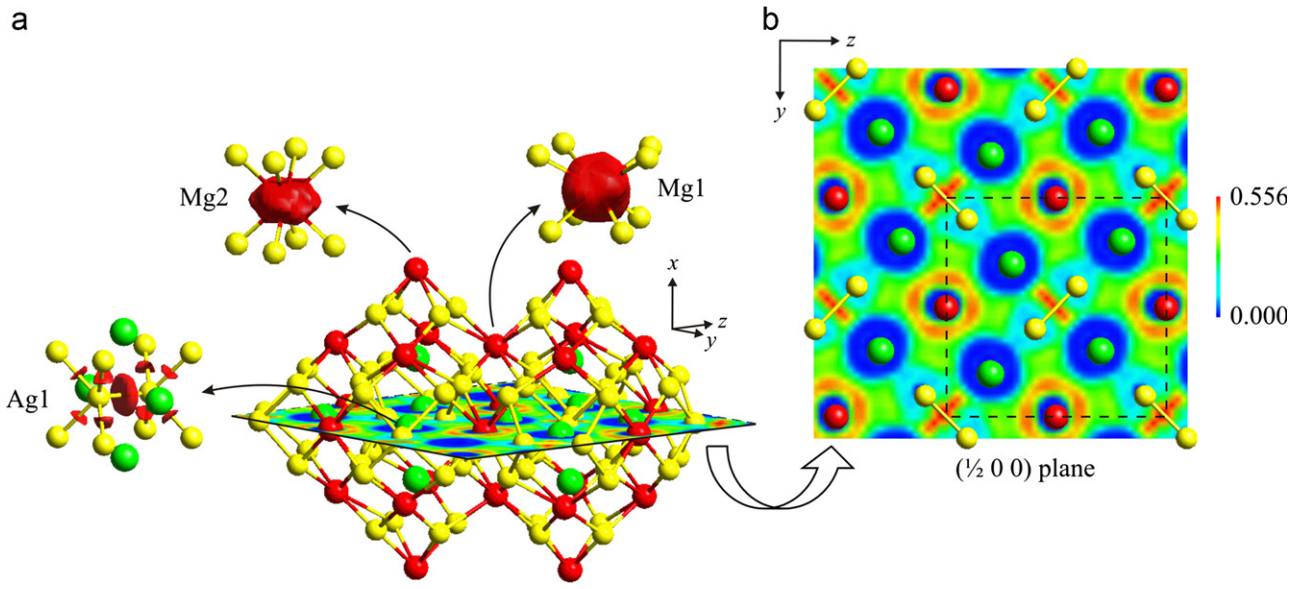

Fig. 3. (a) 3D isosurfaces of the electron localization function ($\eta = 0.8$) within the 3D [Ag–Mg] framework and (b) ELF contour plot for $La_4Ag_{10}Mg_3$ (projected view of the (1/2, 0, 0) basal plane).

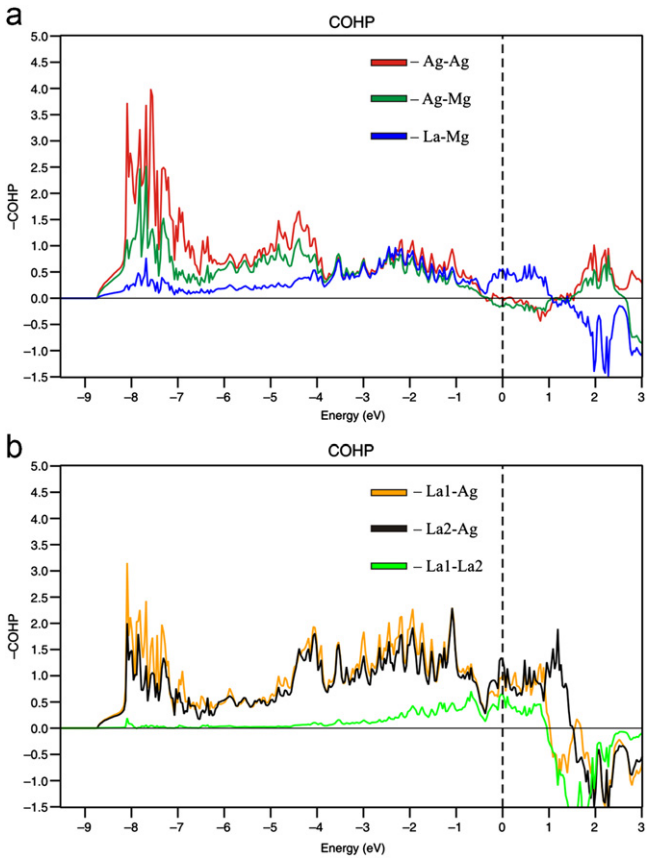

Fig. 4. Crystal orbital Hamilton populations (–COHP) per bond for $La_4Ag_{10}Mg_3$ from LMTO calculations.

coordination polyhedra around the different atom types is not satisfying, moreover the analysis of interatomic distances between Ag and Mg atoms shows the same tendency to contraction (the major part Ag–Mg contacts range from 2.83 to 2.92 Å). The interatomic distances between the other atom types are also comparable to those in $La_4Ag_{10}Mg_3$. Following these characteristics a 3D [Ag–Mg] network containing $[Ag_2Mg_2]$ faces, similar to that in $La_4Ag_{10}Mg_3$, could be evidenced (Fig. 5). In such description the Ag and Mg atoms occupying disordered positions are not included into the network, being displaced into spacious channels along the (100) direction. The remaining La atoms are also located along channels inside the network.

To our knowledge the only compound having similar structure to $La_4Ag_{10.3}Mg_{12}$ is $Sc_4Cu_{14.76}Ga_{7.51}$ [30], which is also classified as a polar intermetallic. These two disordered structures can be described by identical polyanionic 3D frameworks not including the disordered sites, even though the chemical nature of the constituents is strongly different. The main differences between the two structures are the filling of disordering channels along the (100) direction, and the different atoms distribution in the fully occupied sites, resulting in different compositions of the two phases. Electron band calculations performed on an average model of $Sc_4Cu_{14.76}Ga_{7.51}$ showed that disordered positions play an important role in the chemistry of this compound. For this reason a deeper analysis of the chemical bonding in $La_4Ag_{10.3}Mg_{12}$ and searching for relative networks in intermetallics are planned.

4. Conclusions

The two novel $La_4Ag_{10}Mg_3$ and $La_4Ag_{10.3}Mg_{12}$ ternary phases were synthesized and their crystal structures solved from single crystal X-ray data. Crystallographic analysis and electronic structure calculations on $La_4Ag_{10}Mg_3$ ($oS68$-$Ca_4Au_{10}In_3$) reveal substantial Ag–Ag and Ag–Mg bonding within a 3D [Ag–Mg] polyanionic network balanced by La atoms. This phase exhibits the characteristic features of a polar intermetallic according to You et al. [2], showing a sharp distinction between filled bonding states and empty anti-bonding states and the absence of energy gap between the VB and CB.

The $La_4Ag_{10.3}Mg_{12}$ phase represents a new structure type ($oS116$-10.32-$La_4Ag_{10.3}Mg_{12}$) characterized by a large orthorhombic unit cell containing three disordered crystallographic sites of Ag and Mg atoms displaced along the (100) direction. Interatomic distances analysis of this compound highlights strong similarities with $La_4Ag_{10}Mg_3$ including the Ag–Mg contacts contraction. Considering this fact and the similarity with the $Sc_4Cu_{14.76}Ga_{7.51}$

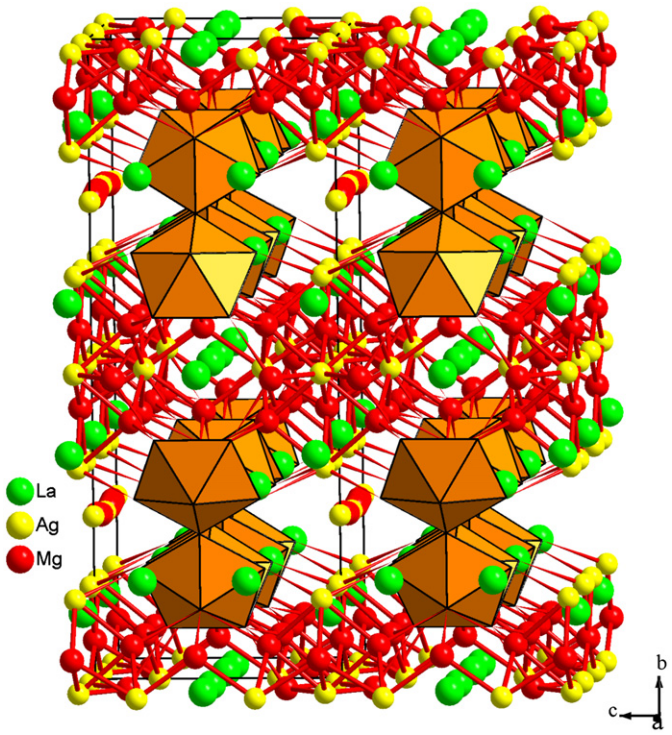

Fig. 5. Crystal structure of $La_4Ag_{10.3}Mg_{12}$ where the 3D [Ag–Mg] network is highlighted (within the framework pentagonal bipyramids of [$Ag4_2Mg11_2Ag12Ag13Mg14$] composition are outlined).

structure, a description of $La_4Ag_{10.3}Mg_{12}$ on the basis of a 3D [Ag–Mg] network is proposed.

The obtained results confirm that Mg atoms can take part in polyanionic networks within polar intermetallic phases [1]. Developing this idea a further investigation of crystal structure and chemical bonding for La–Ag–Mg new ternary phases is in progress.

Appendix A. Supplementary materials

Supplementary data associated with this article can be found in the online version at doi:10.1016/j.jssc.2010.10.018.

References

[1] J.D. Corbett, Inorg. Chem. 49 (2010) 13–28.
[2] T.S. You, P.H. Tobash, S. Bobev, Inorg. Chem. 49 (2010) 1773–1783.
[3] D. Johrendt, G. Kotzyba, H. Trill, B.D. Mosel, H. Eckert, T. Fickenscher, R. Pöttgen, J. Solid State Chem. 164 (2002) 201–209.
[4] A. Saccone, S. De Negri, P. Solokha, in: Proceedings of the XIth IMC, Lviv, 30 May–2 June 2010, L6, p. 8.
[5] SMART, SAINT and SADABS. Bruker AXS Inc., Madison, WI, 2008.
[6] G.M. Sheldrick, SHELXS–97: program for the solution of crystal structures, University of Göttingen, Germany, 1997.
[7] G.M. Sheldrick, SHELXL–97: program for crystal structure refinement, University of Göttingen, Germany, 1997.
[8] O.K. Andersen, Phys. Rev. B 12 (1975) 3060–3086.
[9] H. Skriver, The LMTO Method, Springer-Verlag, Berlin, 1984.
[10] O.K. Andersen, in: P. Phariseau, M. Temmerman (Eds.), The Electronic Structure of Complex Systems, Plenum, New York, 1984.
[11] O.K. Andersen, O. Jepsen, Phys. Rev. Lett. 53 (1984) 2571–2574.
[12] J. Korringa, Physica 13 (1947) 392–400.
[13] W. Kohn, N. Rostoker, Phys. Rev. 94 (1954) 1111–1120.
[14] G. Krier, O. Jepsen, A. Burkhardt, O. K. Andersen, The TB-LMTOASA program, version 4.7, Max-Planck-Institut für Festkörperforschung, Stuttgart, Germany.
[15] U. von Barth, L. Hedin, J. Phys. C 5 (1972) 1629–1642.
[16] P.E. Blöchl, O. Jepsen, O.K. Andersen, Phys. Rev. B 49 (1994) 16223–16233.
[17] R. Dronskowski, P.E. Blöchl, J. Phys. Chem. 97 (1993) 8617–8624.
[18] A.D. Becke, K.E. Edgecombe, Nature 371 (1994) 683–686.
[19] B. Eck, wxDragon 1.6.6, Aachen, 1994-2010, available at 〈http://www.ssc.rwth-aachen.de〉.
[20] Th. Hahn (Ed.), fifth ed., Springer, Dordrecht, The Netherlands, 2005.
[21] P. Villars, K. Cenzual, Pearson's Crystal Data, Release 2009/10, ASM International, Ohio, USA.
[22] M.E. Kirkpatrick, J.F. Smith, W.L. Larsen, Acta Crystallogr. 15 (1962) 894–903.
[23] J.-M. Joubert, R. Černý, K. Yvon, M. Latroche, A. Percheron-Guégan, Acta Crystallogr. C53 (1997) 1536–1538.
[24] Q. Lin, J.D. Corbett, Inorg. Chem. 46 (2007) 8722–8727.
[25] A.L. Spek, PLATON, A Multipurpose Crystallographic Tool, Utrecht University, The Netherlands, 2002.
[26] C. Kudla, Yu. Prots, A. Leineweber, G. Kreiner, Z. Kristallogr. 220 (2005) 102–114.
[27] G. Kreiner, S. Spiekermann, Z. Anorg. Allg. Chem. 627 (2001) 2460–2468.
[28] L. Gelato, E. Parthé, J. Appl. Crystallogr. 20 (1987) 139–143.
[29] P.I. Kryp'yakevitch, in: The Structural Types of the Intermetallic Compounds, Nauka, Moscow, 1997 in Russian.
[30] Q. Lin, S. Lidin, J.D. Corbett, Inorg. Chem. 47 (2008) 1020–1029.